Applied Catalysis B: Environmental 84 (2008) 706–714

Contents lists available at ScienceDirect

Applied Catalysis B: Environmental

journal homepage: www.elsevier.com/locate/apcatb

Factors affecting methanol photocatalytic oxidation and catalyst attrition in a fluidized-bed reactor

Christopher L. Flakker, Darrin S. Muggli *

Department of Chemical Engineering, University of North Dakota, Grand Forks, ND 58202-7101, United States

ARTICLE INFO

Article history:
Received 17 March 2008
Received in revised form 14 May 2008
Accepted 2 June 2008
Available online 11 June 2008

Keywords:
Fluidized bed
Photocatalytic oxidation
Attrition

ABSTRACT

A resolution IV fractional factorial experimental design explored the effects of seven factors on both the methanol photocatalytic oxidation (PCO) rate and the catalyst particle size distribution using a fluidized-bed reactor. The seven factors were as follows: calcination temperature, calcination time, grinding order, particle size, vibration amplitude, carrier gas humidity, and fluidization velocity. Decreasing calcination temperature from 726 to 623 K increased the activity of TiO_2/Al_2O_3 catalysts for methanol PCO. Attrition during fluidization liberated small TiO_2 particles from the bulk catalyst and the rate of attrition increased with gas velocity. Attrition was the primary cause of catalyst elutriation and not the presence of fine particles initially present in the bed from catalyst preparation. Increasing humidity caused agglomeration of fine particles, which reduced the amount of catalyst carryover. Removal of fines from the catalyst bed prior to fluidization caused an increase in catalyst attrition until the amount of fines present in the bed was similar to that of a bed in which fines were not removed.

1. Introduction

Indoor-air pollution is major health risk because people spend 90% of their lives indoors where pollutants such as volatile organic compounds (VOCs) are often at levels several times greater than outside [1–5]. Moreover, people who are most vulnerable to poor air quality (young, elderly, and sick) spend more time indoors compared to the rest of the population [3,5].

Photocatalytic oxidation (PCO) offers a unique solution to mitigate VOC contaminants in indoor air [2,6,7] because it oxidizes many VOCs to CO_2 and H_2O at room temperature [2,8–13]. For indoor-air applications, photocatalytic fluidized-bed reactors possess advantages of high catalyst loadings and high PCO rates as compared to other reactor configurations such as fixed-film and packed-bed reactors [14–16]. Catalysts in fluidized beds, however, are subject to attrition and entrainment in the reactor effluent [17–19]. Successful implementation of a fluidized-bed indoor-air purifier requires developing catalysts that are active, fluidize well, and are entrainment/attrition resistant.

Titanium dioxide (TiO_2) is the most commonly used photocatalyst [8,12,20] because it is suitably active, chemically stable, and non-toxic. Titanium dioxide by itself is a poor choice as a fluidized-bed catalyst due to high carryover rates, attrition, and substantial cohesive forces that cause agglomeration and stagnation in a fluidized bed [21,22]. Titania can be modified, however, to improve its fluidization properties and minimize attrition. Nelson et al. [22] supported TiO_2 on γ-alumina and the resulting catalyst was more active, displayed superior fluidization characteristics, and was more elutriation resistant than Degussa P-25 TiO_2.

This TiO_2/Al_2O_3 study investigates catalyst preparation and fluidized-bed operation parameters and their impact on both PCO and catalyst elutriation rates. The catalyst preparation parameters were as follows: calcination temperature, calcination time, and grinding before or after calcination. Grinding order was an experimental factor because preliminary observations suggested that although grinding before calcination was easier to perform, the resulting catalyst appeared to fluidize more poorly than when the catalyst was ground after calcination. Many studies have observed that as calcination temperature and calcination time increase, TiO_2 surface area decreases with a concomitant growth in crystallite size [8,23–26]. The decrease in surface area is often implicated in the generally observed decrease in TiO_2 activity with calcination temperatures above 773 K [8,24–28]. Two studies observed maximum photoactivity for catalysts calcined at 673 and 623 K, respectively [8,26]. Low calcination temperatures <600 K are not adequate to induce complete crystallization [23,26] and thus yield lower activities.

The fluidized-bed operation parameters investigated in this study were as follows: particle size, vibration amplitude, humidity, and carrier gas velocity. One goal of this study is to determine

* Corresponding author. Tel.: +1 701 777 2337; fax: +1 701 777 3773.
E-mail address: darrin_muggli@und.nodak.edu (D.S. Muggli).

0926-3373/$ – see front matter © 2008 Elsevier B.V. All rights reserved.
doi:10.1016/j.apcatb.2008.06.003

whether catalyst carryover is primarily from fines generated by attrition during fluidization or the elutriation of fines already present in the catalyst bed. Sieving prior to fluidization and omitting the finer particulates (particle size parameter) would help elucidate this point. If carryover is mainly composed of fines present before fluidization, then the particle size factor should have a significant impact on total carryover mass. If carryover is mainly composed of fines generated by attrition, the particle size factor should not change total carryover mass. In addition, particle size was studied because fine particulates tend to agglomerate due to cohesive forces [29,30] and previous work has shown that the agglomeration of fines reduces entrainment and attrition in fluidized beds [17,18].

Gas velocity and vibration amplitude affect directly the intensity of fluidization and could affect overall reaction rate and carryover [17,18]. High and low values of superficial vapor velocity were 2.8 and 2.4 cm/s, respectively. Fluid velocity was included to test for possible mass-transfer limitations as well as determine its effect on catalyst elutriation. Increasing gas velocity increases the number of elutable fines. Increasing gas velocity and vibration amplitude causes catalyst particles to collide with greater force and travel through UV irradiated and "dark" regions with greater frequency. Increasing impact force can increase attrition, and increasing the cycle rate between UV irradiated and "dark" regions could increase overall CO_2 production rates.

High and low values of vibration amplitude were 0.178 and 0.089 μm, respectively. In the current study, vibration amplitude was included as an operation factor because it has not been studied previously and may impact the rate of catalyst attrition. Indeed, vibration has been used previously to improve fluidization [18,21,31]. Vorontsov et al. [21] compared vibrofluidized and multiple fixed-bed photoreactors. Using acetone as the reactant, they showed that a granular vibrofluidized bed (quantum efficiency = 8.7%) was superior to a granular fixed bed (6.9%), which was more active than fixed film (5.9%) and powder (5.8%) beds.

Humidity has been shown to affect the activity of TiO_2 photocatalysts for some reactions [4,27,32] and therefore it was included as an experimental parameter. Moreover, gas-phase H_2O also affects interparticle cohesive forces. Vervoorn [33] observed an abrupt maximum of the cohesive force between TiO_2 particles with increasing humidity at low humidity levels (~2% RH) followed by a general decrease of cohesiveness as relative humidity approached 100%. Fukuoka et al. [34] observed generally that hydrophilic powders (such as TiO_2 [30]) displayed increasing cohesiveness with increasing humidity over all humidity levels studied (40–90% RH). They also found the increase in cohesiveness due to humidity is much more sensitive in fine powders <75 μm than coarse >180 μm. Vorontsov et al. [21] concluded that TiO_2 attrition rates are high at low humidity levels (~0% RH) and increasing humidity decreases attrition in a fluidized-bed scheme. The low and high humidity values in the current study were ~0 and 22% RH.

This study will determine the effects of the above parameters on the methanol PCO and catalyst elutriation rates. Methanol was chosen as a model compound because it is a common indoor-air pollutant that has a high photoefficiency, which makes PCO an attractive method for its removal [35–41]. This study will also determine the source of catalyst carryover; whether or not eluted particles are generated primarily during fluidization or present initially as fines from catalyst preparation. In addition, the composition of eluted catalyst will be determined and compared to the bulk catalyst.

A 16-run screening design investigated the effects of the above seven parameters (factors) on five responses. This fractional factorial design allowed the effects of the seven parameters on each response to be estimated independently. For example, the effect of calcination temperature on the PCO rate could be estimated independently of the effect of calcination time. In this resolution IV design, the main effects of each parameter could be estimated confidently, but the two-factor interactions were confounded with each other. That is, when a two-factor interaction was found to be significant, the interpretation as to which two-factor interaction was important was somewhat indefinite.

2. Experimental methods

2.1. Catalysts

Sixteen batches of supported TiO_2–Al_2O_3 catalyst (30 wt% TiO_2) were prepared using a method similar to that used by Liu et al. [42] and Nelson et al. [22]. Briefly, TiO_2/Al_2O_3 was prepared by mixing ethanol (95 vol.%) and γ-alumina (Aldrich, Brockmann I, Standard Grade), followed by adding slowly the appropriate amount of titanium (IV) butoxide (Aldrich, 97%) to achieve the desired TiO_2 loading [22]. The resulting solution was then heated to 353 K until the liquid evaporated. The resulting solid was dried at 423 K for 4 h and finally calcined at the desired temperature and time. The experimental design called for varying three catalyst preparation factors: calcination temperature (623–723 K), calcination time (3–6 h), and grinding order (before or after calcination). The final catalyst batch mass was ~70 g. Each batch was split into 30 g each of "A" and "B" batches and the remaining 10 g was stored. The A and B samples were sieved to obtain particle size distributions. Large catalyst particles from screen mesh 60 (>250 μm) were removed from all catalyst batches because preliminary experimentation revealed that they caused excessive channeling in fluidized beds.

As listed in the screening design, "coarse" catalyst beds were prepared by removing the contents of the catch pan and screens with mesh sizes of 325 and 270 (and 60) from the catalyst batch. Note that the removed fines were not used in the calculation of mean diameter, variance, or skewness before fluidization. All other catalyst beds were prepared by removing only the contents of screen 60 from the catalyst bed. The average catalyst fines removed was 1.25 g (catalyst in the catch pan, screen 325, and screen 270). The average catalyst mass in screen 60 (>250 μm) was 2.6 g. After sieving and removing the appropriate catalyst particle sizes, catalyst residing in the remaining sieve screens was mixed together.

2.2. Apparatus

The experimental apparatus has been described previously [43]. Briefly, it consisted of a vertical pyrex tube (2 cm i.d.) with a porous frit that supported a bed of TiO_2–Al_2O_3. Twelve black lights (Johnlite, F8T5BLB, 8-W) surrounded the reactor and provided UV radiation. A frequency generator produced a 50 Hz sinusoidal signal that was amplified prior to reaching the vibration generator. The vibration generator oscillated the reactor vertically. High and low levels of vibration corresponded to amplitudes of 0.178 or 0.089 μm, respectively, as measured by a dial caliper.

An air/methanol stream with or without H_2O passed upward through the reactor at a total flow rate of 740 or 860 sccm, dictated by the screening design level for flow rate. Desiccants removed moisture from the house air to near 0% RH. The main air flowed through either a bypass line or a gas bubbler filled with water at 0 °C, depending on whether or not the experimental design called for humidity. The methanol feed concentration was 4000 ppm and the humidity concentration, when present, was 6900 ppm which

corresponds to 22% RH at 298 K. Regardless of flow scheme, reactor effluent passed through two 5 μm particulate filters (SpeedAire #4ZL07) and a 0.5 μm particulate filter (Swagelok #SS-6TF-05). After the filters, the air flowed through the autosampling valve of a SRI 8610C gas chromatograph fitted with a 2.4 m Alltech Hayesep Q 80/100 column. The GC sampled reactor effluent every 30 min and a methanizer/FID arrangement quantified CO_2. Calibration was accomplished by injecting known amounts of CO_2 and methanol at three concentrations for calibration curves.

2.3. Fluidized-bed PCO procedure

Fluidized PCO was performed on the A batch of each catalyst. The catalyst batch was weighed, placed in the reactor, and bed height recorded before each experiment. Methanol and water rotameters were set to flow rates dictated by the screening design (experimental order was fully randomized). Initially the carrier gas flowed downward to saturate the catalyst with methanol prior to switching carrier gas flow direction for fluidization. The down flow arrangement for catalyst bed saturation was required because saturation times varied between catalyst batches. If the catalyst was saturated while fluidized, each catalyst bed would have been fluidized for differing lengths of time. Variation in fluidization duration is undesirable because fluidization impacts the responses studied.

Once the catalyst bed was saturated with methanol, the flow direction reversed to fluidize the bed. The UV lamps and vibration generator were turned on at this time. UV light irradiated the catalyst bed for 4 h, after which the UV lamps were shut off. Fluidization, vibration, and feed air continued for another 2 h for a total of 6 h of fluidization. Production of CO_2 increased initially during fluidized PCO and reached steady state during the final 90 min of UV irradiation. Reaction rates were quantified by averaging the steady-state CO_2 production rates. The CO_2 production rates were normalized by catalyst bed volume to account for CO_2 production differences stemming from differences in total irradiated catalyst area.

After the experiment, all flow rates were returned to zero and the catalyst bed height was recorded and the bed was massed. The particulate filters were disassembled and the catalyst captured from the filters was massed. Fine catalyst particulates (fines) captured in the particulate filters were compiled into two batches based on the level (high or low) of experimental flow rates. Thus, two batches of carryover were acquired, one at low gas flow and one at high gas flow. These eluted fines will be referred specifically as "high flow fines" and "low flow fines," or generally as carryover or eluted fines. The A batch catalysts remaining in the reactor after fluidization will be referred to as "bulk A" catalyst.

After fluidized PCO, the A batches of catalyst were sieved again to quantify changes in particulate distribution due to fluidization. The B catalyst batches were sieved a second time to quantify any changes in particulate distribution due to sieving.

2.4. Catalyst characterization and fixed-bed PCO

X-ray diffraction analysis was performed on eight B catalysts, four samples of carryover, and pure alumina. A Philips ExpertPro X-ray diffractometer with an X celerator detector recorded the diffraction patterns. The X-ray source was Cu Kα and the diffractometer scan range was 5–90° at a rate of 0.2°/s. The 13 spectra were compared to database standards for rutile TiO_2, anatase TiO_2, and Al_2O_3.

Catalyst carryover captured in the particulate filters (SpeedAire) during the fluidization experiments was analyzed by temperature-programmed desorption (TPD) of H_2O and temperature-programmed oxidation (TPO) of methanol. Samples of B catalysts and pure alumina were subjected to TPO. The transient system used for TPO and TPD has been described previously [44]. During TPO, 50 mg of catalyst were placed in a cylindrical quartz reactor fitted with a glass frit. An 80/20% mixture of helium/oxygen flowed through the reactor at 100 sccm. Three injections of methanol (1 μL each) were administered upstream from the catalyst bed to saturate it with methanol. Once the catalyst was saturated and excess methanol was flushed from the gas phase, a furnace heated the catalyst to 723 K at a rate of 1 K/s and held this temperature for 30 min. Oxidation products and methanol desorption were recorded using a Pfeiffer Vacuum Prisma quadrupole mass spectrometer. To perform TPD of H_2O, the above procedure was repeated but using H_2O so saturate the catalyst and 100 sccm He as the carrier gas.

A granular film reactor compared catalyst activities for non-fluidized PCO. The apparatus has been described previously [45]. Bulk A catalysts synthesized with high and low calcination temperature as well as eluted fines were studied in this reactor. Catalyst powder (~0.25 g) was spread over a 63 mm × 57 mm area. An air stream (900 sccm) containing methanol (10 000 ppm) passed over the granular film. UV lights initiated PCO and a gas chromatograph recorded CO_2 production.

3. Results and discussion

Table 1 shows the resolution IV, one-eighth fractional factorial experimental design that was used in this study. Seven factors were studied to determine their effects on five responses. The seven experimental factors were as follows: calcination temperature (X_1), calcination time (X_2), grinding order (X_3), particle size (X_4), vibration amplitude (X_5), carrier gas humidity (X_6), and fluidization velocity (X_7). Two responses, catalyst carryover amount and reaction rate normalized by catalyst volume, were determined during fluidization experiments. Three additional responses (mean diameter, variance, and skewness) were obtained from measuring the changes in the catalyst particle distributions after fluidization. Note that in encoding fluidization velocity, −1 corresponds to the high-flow rate and +1 corresponds to the low-flow rate.

3.1. Reaction rate

Half-normal plots such as Fig. 1 determined if any parameter affected significantly the reaction rate. The abscissa of a half-normal plot is the absolute value of the effect, which in Fig. 1 is the change in reaction rate that resulted from increasing the parameter from its low to high value. For example, Fig. 1 shows that increasing calcination temperature from 623 to 723 K changed reaction rate by 8.3×10^{-9} mol/(min cm^3) catalyst. The corresponding ordinate value is the Z-score, from the standard normal distribution (SND). In Fig. 1, the Z-scores represent the distribution of values that would be expected from a sample size of 15 taken from the SND. Thus, those effects that are only due to random variation, which is normally distributed, will form a straight line through the origin. Effects that are significant would be greater than those expected from random variation and therefore they would appear as outliers (in the upper right of the figure) from the line drawn through the other effects. This analysis is similar to plotting the effects on probability paper.

Fig. 1 shows that the change in calcination temperature (X_1) had the largest effect on the CO_2 formation rate, although the X_1 effect in Fig. 1 is still fairly close to the line. Nelson et al. [22] studied an identical catalyst in a fluidized-bed reactor and found that increasing calcination temperature from 673 to 823 K decreased

Table 1
Fractional factorial experimental design, confounding pattern, and defining relation, used to determine factors which impacted significantly catalyst activity, carryover, and attrition

Catalyst batch	Run	Run order	X_1	X_2	X_3	X_4	X_5	X_6	X_7	X_8	E_1	E_2	E_3	E_4	E_5	E_6	E_7	CO_2 formation rate ($\times 10^8$ mol/(min cm^3(cat)))	Carryover amount (g)
1	1	1	–	–	–	–	–	–	–	–	+	+	+	+	+	+	+	4.1	1.7
2	7	2	–	+	+	–	–	–	+	+	–	–	+	+	+	–	–	3.2	1.6
3	6	3	+	–	+	–	–	+	+	–	–	+	–	–	+	+	–	3.2	1.0
4	8	4	+	+	+	–	+	–	–	–	+	+	–	+	–	–	–	2.2	1.8
5	2	5	+	–	–	–	+	–	+	+	–	–	–	+	–	+	+	1.5	1.4
6	14	6	+	–	+	+	–	–	–	+	–	+	+	–	–	–	+	2.4	1.7
7	4	7	+	+	–	–	–	+	–	+	+	–	–	–	+	–	+	2.7	0.5
8	9	8	–	–	–	+	–	+	+	+	+	+	–	+	–	–	–	3.3	1.0
9	15	9	–	+	+	+	–	+	–	–	–	–	–	+	–	+	+	2.9	1.1
10	13	10	–	–	+	+	+	–	+	–	+	–	–	–	+	–	+	4.0	1.0
11	10	11	+	–	–	+	+	+	–	–	–	–	+	+	+	–	–	2.3	1.3
12	11	12	–	+	–	+	+	–	–	+	–	+	–	–	+	+	–	3.6	2.0
13	16	13	+	+	+	+	+	+	+	+	+	+	+	+	+	+	+	3.0	0.8
14	3	14	–	+	–	–	+	+	+	–	–	+	+	–	–	–	+	3.7	0.4
15	5	15	–	–	+	–	+	+	–	+	–	+	–	+	–	+	–	3.1	1.9
16	12	16	+	+	–	+	–	–	+	–	+	–	+	–	–	+	–	4.1	2.0

Confoundings: $E_1 = 12 + 35 + 47$, $E_2 = 13 + 25 + 47 + 67$, $E_3 = 14 + 27 + 56$, $E_4 = 15 + 23 + 46$, $E_5 = 16 + 37 + 45$, $E_6 = 26 + 34 + 57$, $E_7 = 17 + 24 + 36$; X_1 = calcination temperature, X_2 = calcination time, X_3 = grinding before or after calcinations, X_4 = particle size, X_5 = vibration amplitude, X_6 = humidity, X_7 = fluid velocity. Defining relation: $I = 1235 = 2346 = 1348 = 1247$.

significantly the catalyst activity. The temperatures explored by Nelson et al. (673–823 K) were higher than those in this study (623–723 K) and covered a greater range. Subsequent experimentation using a granular film reactor, presented below, showed conclusively that decreasing calcination temperature (from 723 to 623 K) increased significantly the PCO activity.

Fig. 2a shows the average values for CO_2 production rate at low and high settings of each independent variable studied. In agreement with Figs. 1 and 2a shows that a low value of calcination temperature increased the CO_2 production rate. None of the other factors, however, impacted significantly the CO_2 production rate (Figs. 1 and 2a). Fig. 2a indicates that increasing the fluid velocity *decreased* the CO_2 production rate slightly (Fig. 2). This indicates clearly that this apparent effect of fluid velocity is simply a reflection of the random variation of the system. Moreover, because CO_2 production rate did not increase significantly with fluid velocity, the reactor was not mass-transfer limited. Pore diffusion also did not limit the experiments as the effect of particle size was insignificant. That is, if pore diffusion limited the reaction rate, decreasing particle size would increase the CO_2 formation rate. Fig. 2a shows that the average PCO rate for the coarse bed, indicated by the high level of the particle size variable, was *greater* than that of the fine bed, which shows clearly that this difference was only due to random variation. The fluidized bed appears to be free of detrimental gas channeling, as indicated by the lack of

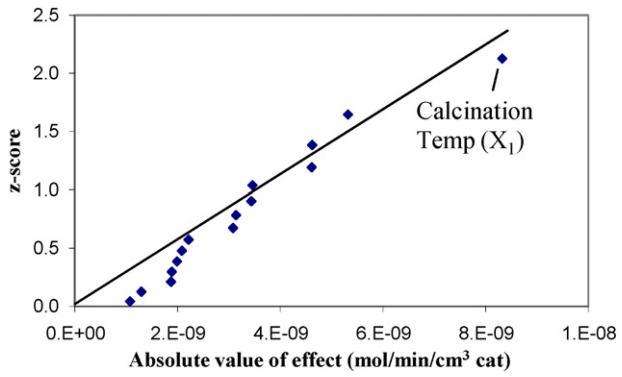

Fig. 1. Half-normal plot of effects on CO_2 production rate normalized by catalyst volume during the screening experiments of A batch (fluidized) catalysts.

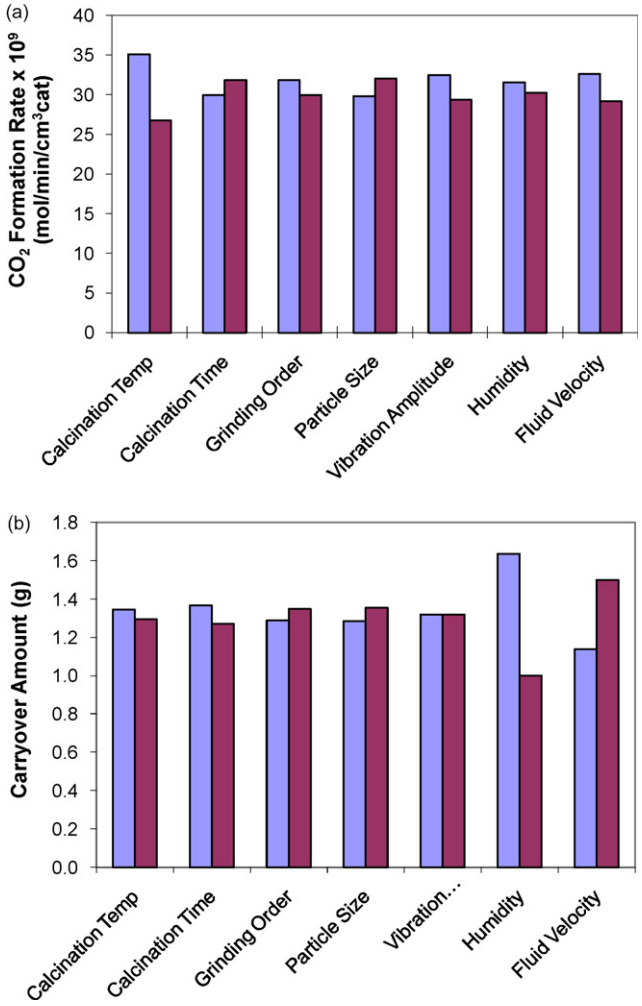

Fig. 2. Average CO_2 production rates (a, top panel) and catalyst carryover amounts (b, bottom panel) for the low (left column) and high (right column) values of the seven catalyst preparation and fluidized-bed operation parameters.

significant impact of vibration amplitude on the CO_2 production rate. Previous experiments (not shown) indicated that too small of a vibration amplitude would not fluidize adequately the bed and lead to excessive channeling. Lastly, Figs. 1 and 2a indicate that at the humidity levels studied, methanol competes effectively with H_2O for active sites. That is, increasing humidity did not reduce significantly the methanol coverage on the active sites for PCO.

Figs. 1 and 2a indicate which catalyst preparation and operating and conditions can be used to maximize reaction rate. Moreover, and equally important, these figures indicate which parameters can be set at their economic minima. For example, the results show that one need not calcine the catalysts for the longer time tested in this study. In addition, smaller vibration amplitudes and fluidization velocities are adequate to ensure adequate fluidization. Finally, a careful particle size selection is not needed to maximize reaction rate. Thus, gaining knowledge of insignificant factors can lead to significant economic advantages.

3.2. Catalyst particle size distribution

When analyzing particle size distribution by sieving the particles, care must be taken to account for the possible reduction in particle size during sieving. To account for this potential experimental artifact, each catalyst was synthesized in quantities that allowed for separation into two batches, denoted "A" and "B". Each A batch was sieved prior to and after this catalyst was fluidized. The sieving was done to quantify the extent of attrition and fines generation that occurred during fluidization. As a control group, each B batch was sieved twice, but the B samples of catalyst were not fluidized. The reason for the B batch was to identify any artifacts in the particle distribution parameters that were not from fluidization but instead were due to attrition that occurred during sieving. If excessive attrition occurred during sieving, the changes in the particle size distribution of the B batch of catalyst could be used to normalize the A batch data and thus segregate the effects of attrition from fluidization and attrition from sieving. Three descriptive parameters were calculated from the particulate distributions: mean diameter, variance, and skewness. Table 2 lists the changes of mean diameter, variance, and skewness between sievings.

Table 2 shows that for the B catalysts, the 95% confidence intervals included zero for the average changes in diameter ($3.6 \pm 3.8\ \mu m$), variance ($-60 \pm 74\ \mu m^2$), and skewness ($(-1.4 \pm 1.6) \times 10^{-6}\ \mu m^{1.5}$). Thus, all three parameters could not be distinguished significantly from zero. In contrast, the same three parameters for the particle size distribution of the A catalysts were all significantly different from zero as shown in Table 2. These results show that the changes in mean diameter, variance, and skewness for the A catalyst samples were not artifacts of sieving but effects of parameters used in the screening experiments and/or fluidization.

At a 95% confidence level, the mean diameter of the A batch of catalyst (subjected to fluidization) decreased significantly between the two sievings whereas the diameter of batch B (no fluidization) did not change significantly (Table 2). A half-normal plot of the change in mean diameter for batch A (not shown) revealed that none of the seven factors affected significantly the mean particle diameter. Because the only difference between A and B batch catalysts was fluidization, which was a factor common to all A batch experiments, it was attributed as the cause of reduction in mean particle diameter. The data were also analyzed by blocking on batches, as another method to isolate the effect of fluidization from that of sieving, with the same results. That is, the blocking analysis analyzed the data differently, to eliminate the effect of the batch-to-batch variation, in an attempt to increase the precision of the results of the analysis. For example, the change in mean diameter for batch 1B was subtracted from that of batch 1A. This computation was performed for all batches and a half-normal plot of the effects, using these differences as the response, showed that none of the factors were significant (even though fluidization itself was significant).

Note that the A batch of catalyst did not include any of the carryover fines during the post-fluidization sieving. Thus, if the fines captured in the carryover filters were due only to those fines initially present in the bed, the mean diameter of A batch catalysts would be *greater* than that of the B batch. The decrease in mean diameter (Table 2) shows clearly that fluidization causes attrition of the TiO_2/Al_2O_3 catalyst. Probability plots of B batch catalysts (not shown) revealed that no factors caused a significant change in mean particle diameter, variance, or skewness. Of note, however, was that the particle size factor (X_4) was nearly significant in reducing skewness and mean particle diameter.

The variance of the particle size distribution increased after fluidization of the A catalysts (Table 2). As mentioned above for mean particle diameter, attrition during fluidization created small particles, which increased the variance of the particle size distribution. Fig. 3 is a half-normal plot of the change in variance

Table 2
Change in catalyst distribution parameters between sieving

Batch #	Mean diameter (μm)		Variance (μm^2)		Skewness ($\mu m^{1.5}$)	
	A	B	A	B	A	B
1	−21	−0.76	520	−94	-3.3×10^{-6}	-2.9×10^{-8}
2	−28	−7.9	490	−81	-1.4×10^{-6}	1.5×10^{-6}
3	0.63	−8.1	130	140	-2.1×10^{-6}	-5.0×10^{-7}
4	−27	3.9	530	−130	-3.0×10^{-6}	6.6×10^{-7}
5	−31	7.8	670	−300	-2.5×10^{-6}	1.4×10^{-6}
6	−17	9.8	510	140	-3.6×10^{-6}	-1.1×10^{-6}
7	−6.1	4.5	−89	−68	1.5×10^{-6}	4.4×10^{-7}
8	−10	5	−54	−310	-4.6×10^{-6}	-1.1×10^{-6}
9	−14	9.8	380	−26	-6.6×10^{-6}	-4.4×10^{-6}
10	−11	3.2	500	90	-5.7×10^{-6}	-4.3×10^{-6}
11	−26	14	480	14	-3.4×10^{-6}	-1.1×10^{-5}
12	−12	−8.2	360	−20	-5.1×10^{-6}	-1.5×10^{-6}
13	1	5.3	93	59	-1.3×10^{-6}	-1.5×10^{-6}
14	−12	−2.2	170	−42	-1.4×10^{-6}	-5.5×10^{-7}
15	−19	9.6	160	−250	2.9×10^{-7}	1.1×10^{-6}
16	−24	11	370	−73	-3.6×10^{-6}	-1.6×10^{-6}
Average with 95% confidence interval	-16 ± 5	3.5 ± 4	330 ± 100	-60 ± 70	$(-2.9 \pm 1) \times 10^{-6}$	$(-1.4 \pm 2) \times 10^{-6}$

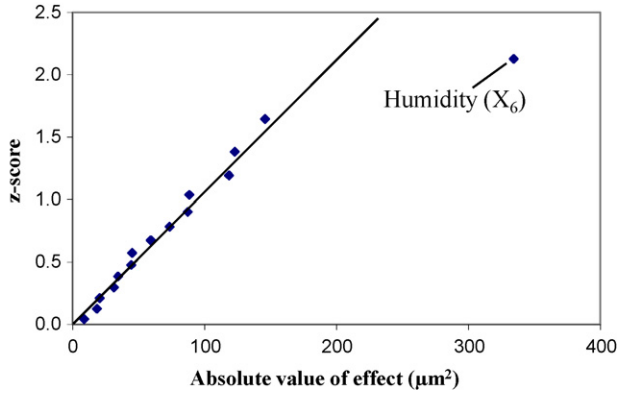

Fig. 3. Half-normal plot of effects that changed variance during fluidization of A batch (fluidized) catalysts.

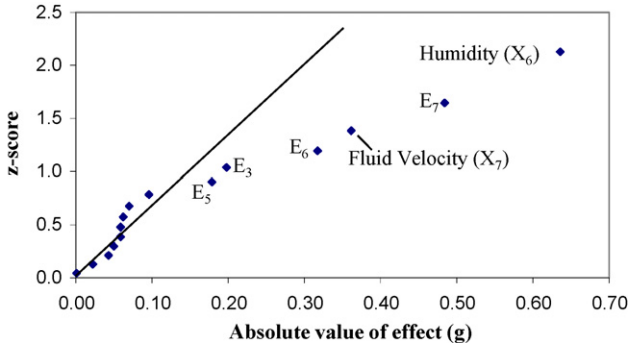

Fig. 5. Half-normal plot of effects that altered total catalyst carryover mass during screening experiments of A batch (fluidized) catalysts.

versus the experimental parameters. It showed that the only significant factor affecting variance was the humidity of the carrier gas during fluidization. The value of humidity's effect was negative, indicating that low levels of humidity (~0% RH) coincided with large increases in the variance of the particulate distributions. Apparently, at high humidity levels, fines agglomerate and behave as larger particles, thus mitigating the increase in variance caused by fluidization. The aforementioned half-normal plot for mean particle diameter showed that humidity had the largest effect on the reduction of mean diameter, although it was not clearly significant. As discussed in more detail below, fines act as lubricants in the fluidized bed and high humidity causes agglomeration of the fines, thus decreasing bed lubricity and thereby increasing the attrition rate.

Table 2 shows that skewness decreased significantly between sievings of A catalysts. This indicates that attrition during fluidization caused particle distributions to become more skewed toward finer particles after fluidization. Fig. 4 shows that the particle sieving factor (X_4, omitting fine particles from the batch) had the largest effect on the change in skewness. The sign of the X_4 effect was negative, which indicates that a coarse initial particle distribution corresponded to a greater *change* in skewness towards finer particles than a natural particle distribution. Because fine particles act as lubricants in fluidized beds [46], their omission from the bed (X_4) increased fine production from attrition. Omitting fines from the beds did not reduce significantly the total amount of carryover (see below). That is, in this experiment removing fines caused increased attrition so that the amount of catalyst carryover did not change significantly. Note that the distribution before fluidization did *not* contain the omitted fines.

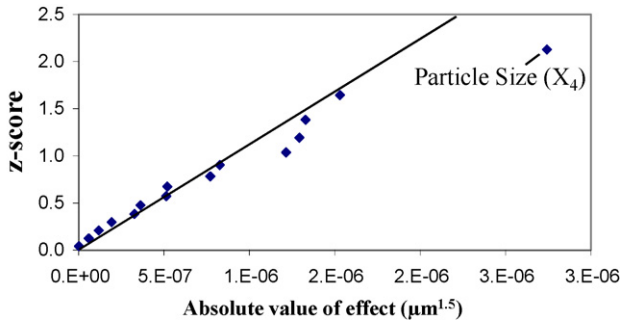

Fig. 4. Half-normal plot of effects that changed skewness during the screening experiments of A batch (fluidized) catalysts.

3.3. Elutriation

Catalyst beds were massed before and after fluidization and the difference in mass determined the amount of eluted catalyst (carryover). Although catalyst captured in the particulate filters was also massed, at low flow rates catalyst accumulated in the tubing between the reactor and particulate filters so that the amount captured depended on flow rate. Therefore, the difference in catalyst bed mass, instead of the amount collected in the filters, quantified catalyst carryover. Fig. 2b shows the average carryover amounts determined for each independent variable studied.

Fig. 5 is a half-normal plot of the absolute value of each effect versus normal score, using catalyst carryover amount as the response. Note that the particle distribution factor (X_4) was not a significant effect in Fig. 5. That is, removing of fines from the bed prior to fluidization did not change the amount of catalyst that eluted from the bed. The amount of fines removed prior to fluidization (1.3 ± 0.7 g) was equal to the average amount of carryover collected (1.3 ± 0.3 g) so that if catalyst carryover was due mainly to elutriation of fines initially present in the bed, the particle distribution factor should have had a dramatic effect on the amount of carryover collected. Thus, the absence of the particle distribution factor from the significant effects indicates that fines originally present in the bed are not a significant part of carryover and that carryover fines are products of attrition.

As expected, increasing gas velocity (X_7) increased the catalyst elutriation rate (Fig. 2b). Greater gas velocities increase catalyst attrition as well as allow larger particles to be eluted from the bed. In these experiments, the main effect of gas velocity appears to be an increase in catalyst attrition rate, as the eluted fines were markedly smaller than catalyst that remained in the bed after fluidization. This is supported, at least qualitatively, in the attempted sieving of the carryover particles; because of their small size, they adhered to the sieve walls and could not be sieved effectively whereas none of the bulk particles adhered to the screen surfaces.

Humidity (X_6) had the largest effect on carryover rate (E_7 is confounded by the following two-level interactions: 17, 24, and 36). The value of the humidity effect was negative, indicating that the presence of humidity decreased overall carryover. The effect of humidity on the carryover amount is also shown clearly in Fig. 2b. Humidity may have decreased carryover either by H_2O adsorption on the fines increasing their mass, or by increasing the cohesive forces between particles that causes agglomeration of fines.

Three water TPDs were performed on high and low flow elutriated catalyst to determine if water adsorption could impact significantly the apparent catalyst density and thus affect entrain-

Table 3
Water coverage on high and low flow fine catalysts recorded by TPD

Catalyst	Species	Coverage (μmol/g(cat))	Mass H_2O/mass catalyst
Low flow fines	H_2O	1300 ± 200	0.024 ± 0.004
High flow fines	H_2O	1200 ± 200	0.023 ± 0.003

ment. Table 3 shows that saturating the catalyst fines with H_2O increased their mass by only ~2 wt%. The gas velocity during a low flow rate experiment (2.4 cm/s) corresponds to the terminal velocity of a spherical catalyst particle 0.483 μm in diameter. A 2% increase in density decreased the terminal diameter of catalyst by 1% from 0.483 to 0.477 μm. Thus, an increase in particle mass by water adsorption does not affect significantly the number of elutable fines present in a catalyst bed and therefore should not affect the total carryover mass. Rather, humidity appears to reduce entrainment by promoting agglomeration of fine particles.

The increased cohesiveness of fine particulates with humidity has been observed by others [30,33,34]. Fukuoka et al. [34] demonstrated that as particle size decreases, cohesive forces between particles become increasingly sensitive to humidity level. Matsuda et al. [14] observed a similar phenomenon with ultrafine TiO_2 particles <10 nm; the ultrafine particles agglomerated so strongly that they exhibited a lower entrainment rate than larger (~200 nm) particles. They attributed the lower entrainment rate entirely to the cohesiveness of the fine particles. Because they used ambient air for fluidization, however, particle agglomeration was most likely due to a combination of humidity and small particle size.

3.4. X-ray diffraction

The mass of catalyst carryover captured in the particulate filters was too small to warrant storing each experiment individually, so it was grouped into two batches based on whether it was carryover from high- or low flow rate experiments. The carryover was grouped this way because it was expected that flow rate would be a significant factor on total carryover mass. The carryover was sieved but was so cohesive that it plugged the sieve screens and adhered to the sides of the sieve trays. Thus, the particulate distribution of the carryover could not be determined.

X-ray diffraction methods were used to compare the structure of the catalyst carryover; to determine whether or not it was composed mainly of TiO_2, Al_2O_3, or it was similar to the composition of the bulk TiO_2/Al_2O_3 catalyst. Thus, XRD spectra were compared for the high- and low flow carryover, bulk B catalyst (not fluidized), and Al_2O_3 support used in catalyst preparation. The screening design used to study CO_2 production rate and carryover contained a full factorial in three catalyst preparation factors: calcination temperature, calcination time, and particulate distribution. That is, a full factorial in the above three catalyst preparation factors was analyzed using XRD spectra as the response.

The diffraction patterns of the eight samples that correspond to a full factorial in factors that may affect catalyst structure (bulk B catalyst) were nearly identical. Fig. 6 shows XRD spectra from: the

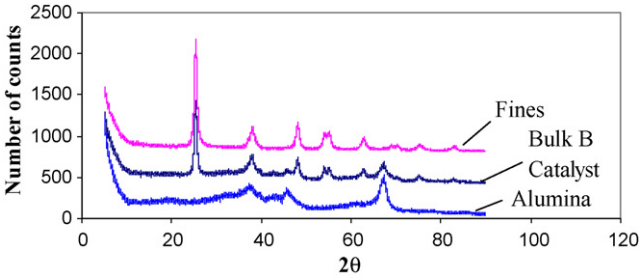

Fig. 6. X-ray diffraction pattern of the Al_2O_3 support used in catalyst preparation, a representative diffraction pattern of the eight bulk catalyst samples and a representative spectra of the catalyst that eluted during fluidization.

Al_2O_3 support used in catalyst preparation, a representative diffraction pattern of the eight bulk catalyst samples, and a representative spectra of the catalyst that eluted during fluidization. All eight bulk TiO_2/Al_2O_3 catalysts (as opposed to eluted catalyst) samples displayed strong anatase peaks and complementary Al_2O_3 peaks.

The diffraction patterns of the four eluted catalyst samples were not different from each other and are represented by a single spectrum. The carryover spectra had strong anatase peaks but lacked the Al_2O_3 peaks at 46° and 67°. The absence of peaks at 46° and 67° indicates that the carryover was predominately composed of anatase TiO_2 formed by attrition during fluidization. Anatase TiO_2 and alumina both have peaks at 38° and thus for the eluted catalyst, the peak in Fig. 6 at 38° is attributed to anatase because the alumina peaks at 46° and 67° are absent.

The average carryover was approximately 5% of the total bed mass. Taking into account the bulk catalyst TiO_2 loading of 30 wt%, catalyst carryover accounts for 16% of the total TiO_2 present in a 26.6 g bed of TiO_2–Al_2O_3. Interestingly, CO_2 production rate did not decrease during the 4-h fluidized PCO. Rutile peaks were not observed for any of the 12 catalyst samples. The calcination temperatures used were below the rutile formation temperature, in agreement with previous studies [23,24,27,28,47,48].

3.5. Temperature-programmed oxidation and desorption

The XRD spectra discussed above indicated that catalyst carryover was primarily anatase TiO_2. A set of confirmation experiments was performed using temperature-programmed oxidation of methanol (Table 4). If the fines were primarily anatase TiO_2, the product distribution from TPO should correspond to TiO_2 more than that of the Al_2O_3 support. In addition, because the screening experiment showed that calcination temperature had the largest effect on reaction rate, TPOs were performed for high and low calcination temperature bulk B catalysts.

During TPO, catalyst fines produced the largest amount of oxidation products (CO and CO_2) followed by the bulk B catalysts and alumina. Total amounts of oxidation products of high and low flow fines could not be distinguished at a 95% confidence level and were combined to give a total CO and CO_2 production amounts of

Table 4
Methanol, CO_2, and CO coverages in (μmol/g cat) recorded during TPO of bulk B catalyst and fines elutriated during screening experiments

Species	Low flow rates	High flow rates	Low calcination temperature	High calcination temperature	Alumina
CO	100 ± 30	100 ± 10	65 ± 2	82 ± 5	44 ± 7
CO_2	160 ± 60	160 ± 20	34 ± 3	26 ± 2	19 ± 5
MeOH	200 ± 90	310 ± 20	310 ± 10	310 ± 20	410 ± 60
Total	500 ± 200	570 ± 50	410 ± 10	420 ± 30	470 ± 70

Table 5
CO_2 production rates of high and low temperature bulk A catalysts and eluted catalyst fines

Catalyst	CO_2 production rate ($\times 10^7$ mol/(min g(cat)))
High flow fines	9 ± 1
Low calcination temperature	7.2 ± 0.3
High calcination temperature	6.0 ± 0.3

250 ± 60 μmol/g catalyst. Total amounts of oxidation products of bulk B catalysts could not be distinguished at a 95% confidence level and were combined to give a total CO and CO_2 production of 100 ± 7 μmol/g catalyst. Total amounts of oxidation products formed during TPO of alumina were 60 ± 10.

Using the Bonferroni method (a comparative *t*-test that corrects, conservatively, for the fact that more than two comparisons are being made) for the following comparisons, the bulk B catalyst produced more CO and CO_2 than did the Al_2O_3 support, due to the presence of TiO_2. The catalyst carryover produced significantly more CO and CO_2 than did the bulk B catalyst, presumably because the fines were primarily TiO_2, in agreement with XRD results. Both comparative tests had confidence levels greater than 99%.

3.6. Granular film reactor

Fig. 1 shows, in contrast to previous results [22] that used a different temperature range, that although calcination temperature had the largest effect on PCO activity for the fluidized-bed screening experiments, the significance of its effect was not clear at the level of precision of the screening experiment. Thus, further testing of the effect of calcination temperature on PCO activity was warranted. Three catalysts were studied using a granular film PCO reactor: high flow fines, high calcination temperature bulk A catalyst, and low calcination temperature bulk A catalyst. Eluted catalyst fines were studied because XRD and TPO analyses showed that fines are mainly TiO_2. Table 5 lists the CO_2 production rates observed for the three catalysts in the granular film reactor.

Using the Bonferroni method, comparative tests showed with 95% confidence that the low calcination temperature catalyst was more active for PCO than the high calcination temperature catalyst. High flow fines had the largest PCO activity (measured as the CO_2 production rate) of the three catalyst studied. A comparative test showed with 95% confidence that the high flow fines have a higher photoactivity than the low calcination temperature catalyst. Thus, these results indicate that decreasing calcination temperature over the range of temperatures studied increases PCO activity. Moreover, the eluted catalyst (primarily TiO_2) was more active than the bulk TiO_2/Al_2O_3 catalysts presumably due to the greater TiO_2 content.

4. Conclusions

Over the ranges studied, decreasing calcination temperature from 723 to 623 K increased catalyst activity. Attrition during fluidization reduces the particle size of TiO_2/Al_2O_3 and catalyst carryover was due to fines produced during fluidization rather than fines present in the bed from catalyst preparation. These fines were primarily composed of TiO_2. Increasing humidity caused agglomeration of fine particles, which reduced the amount of catalyst carryover. Removal of fines from the catalyst bed prior to fluidization caused an increase in catalyst attrition until the amount of fines present in the bed was similar to that of a bed in which fines were not removed.

Acknowledgments

This project was funded in part by the U.S.D.A. Advanced Housing Research Coalition administered by the Forest Product Laboratory. Acknowledgement is made to the Donors of the Petroleum Research Fund, administered by the American Chemical Society (Grant #38906-B5S), and the National Science Foundation (Grants #CTS-0223008 and CBET-0651058). CLF gratefully acknowledges support from the National Science Foundation Research Experience for Undergraduates program (Grant #0243832).

References

[1] C.H. Ao, S.C. Lee, J.C. Yu, Journal of Photochemistry and Photobiology A: Chemistry 156 (2003) 171–177.
[2] F.B. Li, X.Z. Li, C.H. Ao, S.C. Lee, M.F. Hou, Chemosphere 59 (2005) 787–800.
[3] EPA, The Inside Story: A Guide to Indoor Air Quality, United States Environmental Protection Agency and the United States Consumer Product Safety Commission, 1995.
[4] W.-K. Jo, K.-H. Park, Chemosphere 57 (2004) 555–565.
[5] E. Ilgen, N. Karfich, K. Levsen, J. Angerer, P. Schneider, J. Heinrich, H.E. Wichmann, L. Dunemann, J. Begerow, Atmospheric Environment 35 (2001) 1235–1252.
[6] H. Yu, S.C. Lee, J. Yu, C.H. Ao, Journal of Molecular Catalysis A: Chemical 246 (2006) 206–211.
[7] K.-P. Yu, G.W.-M. Lee, W.-M. Huang, C.-C. Wu, C.-l. Lou, S. Yang, Journal of the Air & Waste Management Association 56 (2006) 666–674.
[8] A.V. Vorontsov, D.V. Kozlov, P.G. Smirniotis, V.N. Parmon, Kinetics and Catalysis 46 (2005) 189–203.
[9] H.E. Khalifa, ASHRAE Transactions 111 (2005) 535–542.
[10] D.Y. Goswami, D.M. Trivedi, S.S. Block, Journal of Solar Energy Engineering 119 (1997) 92–96.
[11] T.K. Goswami, S.K. Hingorani, H. Greist, D.Y. Goswami, S.S. Block, Journal of Advanced Oxidation Technologies 4 (1999) 185–188.
[12] D.Y. Goswami, Journal of Solar Energy Engineering 125 (2003) 359–365.
[13] M.L. Sauer, D.F. Ollis, Journal of Catalysis 149 (1994) 81–91.
[14] S. Matsuda, H. Hatano, A. Tsutsumi, Chemical Engineering Journal (Lausanne) 82 (2001) 183–188.
[15] R. Nelson, Photocatalytic Oxidation of Methanol in a Fluidized Bed Application, Chemical Engineering, University of North Dakota, Grand Forks, 2004, p. 140.
[16] A.V. Vorontsov, D.V. Kozlov, P.G. Smirniotis, V.N. Parmon, Kinetics and Catalysis 46 (2005) 437–444.
[17] K. Smolders, J. Baeyens, Powder Technology 92 (1997) 35–46.
[18] D. Santana, J.M. Rodriguez, A. Macias-Machin, Powder Technology 106 (1999) 110–118.
[19] J. Werther, J. Reppenhagen, AIChE Journal 45 (1999) 2001–2010.
[20] J. Disdier, P. Pichat, D. Mas, Journal of the Air & Waste Management Association 55 (2005) 88–96.
[21] A.V. Vorontsov, E.N. Savinov, P.G. Smirniotis, Chemical Engineering Science 55 (2000) 5089–5098.
[22] R.J. Nelson, C.L. Flakker, D.S. Muggli, Applied Catalysis B: Environmental 69 (2007) 189–195.
[23] J. Yu, H. Yu, B. Cheng, C. Trapalis, Journal of Molecular Catalysis A: Chemical 249 (2006) 135–142.
[24] Y. Chen, D.D. Dionysiou, Journal of Molecular Catalysis A: Chemical 244 (2006) 73–82.
[25] S.-K. Joung, T. Amemiya, M. Murabayashi, K. Itoh, Applied Catalysis A: General 312 (2006) 20–26.
[26] X. You, F. Chen, J. Zhang, Journal of Sol–Gel Science and Technology 34 (2005) 181–187.
[27] S.-J. Kim, S.-D. Park, Y.H. Jeong, S. Park, Journal of the American Ceramic Society 82 (1999) 927–932.
[28] J. Ovenstone, K. Yanagisawa, Chemistry of Materials 11 (1999) 2770–2774.
[29] A. Castellanos, Advances in Physics 54 (2005) 263–376.
[30] P.A. Hartley, G.D. Parfitt, L.B. Pollack, Powder Technology 42 (1985) 35–46.
[31] E. Jaraiz, S. Kimura, O. Levenspiel, Powder Technology 72 (1992) 23–30.
[32] C.-P. Chang, J.-N. Chen, M.-C. Lu, Journal of Environmental Science and Health, Part A: Toxic/Hazardous Substances & Environmental Engineering 38 (2003) 1131–1143.
[33] P.M.M. Vervoorn, Colloids and Surfaces 25 (1987) 145–154.
[34] E. Fukuoka, S. Kimura, M. Yamazaki, T. Tanaka, Chemical & Pharmaceutical Bulletin 31 (1983) 221–229.
[35] D.S. Muggli, M.J. Odland, L.R. Schmidt, Journal of Catalysis 203 (2001) 51–63.
[36] R.M. Alberici, W.E. Jardim, Applied Catalysis B: Environmental 14 (1997) 55–68.
[37] S.A. Larson, J.A. Widegren, J.L. Falconer, Journal of Catalysis 157 (1995) 611–625.
[38] Y.C. Liu, G.L. Griffin, S.S. Chan, I.E. Wachs, Journal of Catalysis 94 (1985) 108–119.
[39] N.N. Lichtin, M. Avudaithai, E. Berman, A. Grayfer, Solar Energy 56 (1996) 377–385.
[40] C.C. Chuang, C.C. Chen, J.L. Lin, Journal of Physical Chemistry B 103 (1999) 2439–2444.

[41] S.B. Kim, H.T. Hwang, S.C. Hong, Chemosphere 48 (2002) 437–444.
[42] X. Liu, Y. Liu, X. Li, S. Xiang, Y. Zhang, P. Ying, Z. Wei, C. Li, Applied Catalysis A: General 239 (2003) 279–286.
[43] R.J. Nelson, C.F. Flakker, D.S. Muggli, Applied Catalysis B: Environmental 69 (2007) 189–195.
[44] A.C. Lukaski, Transient Photocatalytic Oxidation Study of Organics on Titanium Dioxide Using Mass Spectrometry and Fourier Transform Infrared Spectroscopy, Chemical Engineering, University of North Dakota, Grand Forks, 2003 , p. 162.
[45] S. Miksche, Optimum Photodeposition Parameters for the Production of Ag–TiO_2 and Ag–TiO_2–Al_2O_3 for Photocatalytic Oxidation Applications, Chemical Engineering, University of North Dakota, Grand Forks, 2005, p. 110.
[46] D. Kunii, Levenspiel, Octave, Fluidization Engineering, Butterworth-Heinemann, Stoneham, 1991.
[47] Y.-M. Lin, Y.-H. Tseng, J.-H. Huang, C.C. Chao, C.-C. Chen, I. Wang, Environmental Science and Technology 40 (2006) 1616–1621.
[48] G. Colon, M.C. Hidalgo, G. Munuera, I. Ferino, M.G. Cutrufello, J.A. Navio, Applied Catalysis B: Environmental 63 (2006) 45–59.